Journal Pre-proof

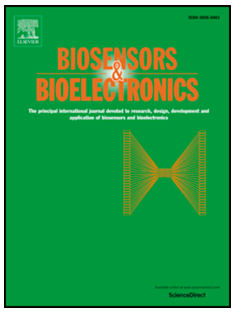

Dual signal amplification by polysaccharide and eATRP for ultrasensitive detection of CYFRA 21–1 DNA

Liying Zhao, Huaixia Yang, Xiaoke Zheng, Jinge Li, Lihe Jian, Weisheng Feng, Jinming Kong

PII: S0956-5663(19)30974-1

DOI: https://doi.org/10.1016/j.bios.2019.111895

Reference: BIOS 111895

To appear in: *Biosensors and Bioelectronics*

Received Date: 20 October 2019

Accepted Date: 14 November 2019

Please cite this article as: Zhao, L., Yang, H., Zheng, X., Li, J., Jian, L., Feng, W., Kong, J., Dual signal amplification by polysaccharide and eATRP for ultrasensitive detection of CYFRA 21–1 DNA, *Biosensors and Bioelectronics* (2019), doi: https://doi.org/10.1016/j.bios.2019.111895.

Credit Author Statement

Liying Zhao**:** Investigation, Writing-original draft, Writing-review & editing

Huaixia Yang: Funding acquisition, Supervision, Writing-review & editing

Xiaoke Zheng: Methodology, Writing-review & editing

Jinge Li**:** Formal analysis, Conceptualization

Lihe Jian: Investigation; Picture

Weisheng Feng**:** Funding acquisition, Methodology, Project administration

Jinming Kong: Funding acquisition, Project administration, Writing-review & editing

Dual signal amplification by polysaccharide and eATRP for ultrasensitive detection of CYFRA 21-1 DNA

Liying Zhao[a], Huaixia Yang[a,*], Xiaoke Zheng[a], Jinge Li[a], Lihe Jian[a],

Weisheng Feng [a,*], Jinming Kong[b,*]

[a] *Pharmacy College, Henan University of Chinese Medicine, Zhengzhou 450046, P. R. China*

[b] *School of Environmental and Biological Engineering, Nanjing University of Science and Technology, Nanjing 210094, P. R. China*

*Corresponding author

E-mail address: yhx998@hactcm.edu.cn, fwsh@hactcm.edu.cn, j.kong@njust.edu.cn

ABSTRACT

Cytokeratin fragment antigen 21-1 (CYFRA 21-1) DNA is a crucial biomarker closely associated with non-small cell lung cancer. Here, we fabricated a novel electrochemical biosensor for ultrasensitive detection of CYFRA 21-1 DNA via polysaccharide and electrochemically mediated atom transfer radical polymerization (eATRP) dual signal amplification. Specifically, thiolated peptide nucleic acid (PNA) probes at 5'-terminals are immobilized on the gold electrode surface for specific recognition of CYFRA 21-1 DNA (tDNA). After hybridization, hyaluronic acid (HA) is linked to the hybridized PNA/DNA duplexes via the recognized carboxylate-Zr^{4+}-phosphate chemistry. Then multiple initiators of the polymerization reaction are introduced via esterification reaction. Lastly, large numbers of electro-active monomers are successfully grafted from the initiation sites of functionalized HA by eATRP reaction, significantly amplifying the electrochemical signal. Under optimal conditions, the constructed sensor can detect as low as 9.04 aM tDNA. Further, this proposed biosensor can also be applied to the direct detection of double-stranded DNA (dsDNA), obtaining 0.12 fM as the detection limit. Besides, this strategy shows high selectivity for mismatched bases and excellent applicability for CYFRA 21-1 DNA detection in the serum samples. Given its high sensitivity, selectivity, ease of operation, low cost and environmental friendliness, this biosensor has considerable potential in early diagnosis and biomedical application.

Keywords: Biosensor; CYFRA 21-1 DNA; Hyaluronic acid; eATRP; Signal amplification

1. Introduction

Lung cancer is characterized by malignant cell growth and is a major threat to human health worldwide. It is mainly classified into small cell lung cancer (SCLC) and non-small cell lung cancer (NSCLC) (Arya and Bhansali, 2011; Hu et al., 2018). In 1993，cytokeratin fragment antigen 21-1 (CYFRA 21-1) was first considered as a sensitive and specific biomarker of NSCLC (Pujol et al., 1993). Currently, identifying biomarkers at the genetic level is of great significance for early diagnosis and monitoring therapeutic efficacy of cancers (Zhao et al., 2018). Several studies have demonstrated that the level of CYFRA21-1 DNA in NSCLC patients is closely associated with disease diagnosis and prognosis (Cedres et al., 2011).

During the past decade, various strategies have been reported for detecting cancer biomarkers, such as immunocytochemistry (Kim et al., 2011), surface plasmon resonance (SPR) (Yang et al., 2017), enzyme-linked immunosorbent assay (ELISA) (Han et al., 2013), electrochemical DNA biosensor (Chen et al., 2018) and electrochemical immunoassay (Zeng et al., 2018). Among these strategies, the electrochemical DNA biosensor has received considerable attention because of its inherent merits of high sensitivity, rapid response, relatively low cost and good portability. Lung cancer is often silent in the early stage and then diagnosed in the advanced stage, where treatment effect may be poor (Srinivas et al., 2001). However, conventional electrochemical method based on 1:1 target-to-signal hybridization ratio limits the sensitivity and applicability of the electrochemical DNA biosensor. Therefore, there is an urgent and significant need to develop a highly sensitive method for CYFRA21-1 DNA detection.

To ensure higher sensitivity, several amplification strategies have been previously proposed, such as biological enzymes catalysis (Shen et al., 2015), nanoparticles (Li et al., 2015) and long chain polymers (He et al., 2019). However, the high cost of enzymes and the laborious and time-consuming operation of nanomaterials limit their application scope. Polymer-based amplification technique is a low-cost, simple and efficient method

that utilizes the dynamic growth of a long chain polymer from one initiation event (Allen et al., 2019). At present, atom transfer radical polymerization (ATRP) is recognized as the most effective method for the synthesis of polymers. ATRP is a controlled/living polymerization technique first reported by Wang and Matyjaszewski in 1995 (Wang and Matyjaszewsk, 1995). Its effectiveness of ATRP is owing to its wide range of available monomers, moderate polymerization temperature and mild reaction conditions. By establishing a dynamic equilibrium between active species at a low concentration and dormant species at a much higher concentration, ATRP can be successfully used for the simultaneous growth of each polymer with well-defined compositions and architectures (Seidi et al., 2018). However, the high catalyst concentration required in ATRP results in low activity of early catalyst and radical termination events. As a result, by adding reducing reagents (e.g. elemental copper, ascorbic acid and hydrazine), activators regenerated by electron transfer ATRP (ARGET-ATRP) method has been developed to trigger ATRP at low catalyst concentration (below 100 ppm) that can also be used to eliminate oxygen (Jones et al., 2018; Leophairatana et al., 2017; Magenau et al., 2013). However, the byproducts of activators regeneration in ARGET ATRP may be poisonous (e.g. dehydroascorbic acid and Sn^{4+} compounds), resulting in an unnecessary color change of the synthesized polymers (Chmielarz et al., 2017; Magenau et al., 2013; Sun et al., 2016). To overcome this limitation, Matyjaszewski et al. developed electrochemically mediated ATRP (eATRP), wherein electrons are used as reducing agents to avoid the formation of reaction byproducts (Chmielarz et al., 2017; Magenau et al., 2011). In comparison with previous ATRP approach, eATRP is a more effective and environmentally friendly method for the synthesis of polymers.

Recently, we verified that eATRP is an efficient and economical signal amplification technology for DNA detection (Hu et al., 2017). The detected sensitivity is closely related to the amount of polymers grafted from the electrode surface. Generally, the total amount of grafted polymers can be increased by generating a relatively longer polymer chain or

more polymer chains on reactive surface sites (Qian and He, 2010). While the former is operationally simple (increasing reaction time or reaction rate), it often leads to non-specific adsorption because the polymerization is not properly controlled. The latter is achieved by increasing the amount of initiators bound to the target molecules. Increasing the amount of polymer chains is an effective method that does not require significant modification to the previous experimental conditions.

Polysaccharide and their derivatives have received extensive attention in the biosensor field owing to their remarkable molecular structure, functional properties, excellent biocompatibility, biodegradability, and nontoxicity (Seidi et al., 2018; Xing et al., 2012). In particular, hyaluronic acid (HA), a naturally anionic biopolymer comprising N-acetyl-D-glucosamine and D-glucuronic acid, contains numerous repeated oxygen-containing functional groups that provide more active sites for labelling signal probes. As a macromolecular initiator, functional HA can make biosensor more sensitive and environmentally friendly. To the best of our knowledge, the strategy of combining polysaccharide and eATRP dual amplification for DNA detection has not been reported so far.

Here, we describe a novel electrochemical biosensor that exploits dual signal amplification through polysaccharide and eATRP for CYFRA 21-1 DNA detection. The ultrasensitive detection of CYFRA 21-1 DNA involves 1) immobilization of thiolated PNA at 5'-terminals onto a gold electrode surface via the self-assembly of Au–S bond; 2) specific recognition of target CYFRA 21-1 DNA with PNA forming a stable PNA/DNA duplexes; 3) attachment of HA to the duplexes via the recognized carboxylate-Zr^{4+}-phosphate chemistry; 4) introduction of multiple initiators of polymerization reaction via esterification reaction and 5) grafting of large numbers of electro-active materials from the initiation sites of functionalized HA by eATRP reaction, thereby distinctly amplifying the electrochemical signal. Using dual signal amplification strategy, the proposed biosensor obtains 1000-fold higher CYFRA 21-1 DNA detection

than that achieved by nanoparticles-based amplification (Chen et al., 2018). Moreover, owing to its merits of high sensitivity, selectivity, ease of operation, low cost, and environmental friendliness, this amplification strategy can be extended to the detection of other types of trace level DNA, holding great potential in biomedical application.

2. Experimental

2.1 Materials and reagents

6-mercapto-1-hexanol (MCH), hyaluronic acid (HA), ferrocenylmethyl methacrylate (FMMA), N-(3-dimethylaminopropyl)-N'-ethylcarbodiimide hydrochloride (EDC), N-hydroxysuccinimide (NHS), 2-bromo-2-methylpropionic acid (BMP), and tris (2-dimethylaminoethyl) amine (Me_6TREN) were obtained from Sigma-Aldrich (St. Louis, USA). Zirconyl chloride octahydrate ($ZrOCl_2 \cdot 8H_2O$), potassium hexafluorophosphate (KPF_6), and lithium perchlorate ($LiClO_4$) were purchased from J&K Scientific Ltd. (Shanghai, China). Diethylamine (DEA) was obtained from Aladdin Industrial Inc. (Shanghai, China). Copper (II) bromide ($CuBr_2$) and potassium bromide (KBr) were purchased from Sinopharm Chemical Reagent Co., Ltd. (Shanghai, China). All other chemical reagents were of analytical purity grade and used without further purification. Normal human serum was supplied by Yu Duo Co., Ltd. (Shanghai, China). Ultrapure water (resistivity ≥ 18.25 MΩ) from a Millipore filtration system was used in all experiments.

PNA probes were tailor-made and purified by Panagene Inc. (South Korea). All synthetic oligonucleotides were purchased from Sangon Biotechnology Co. Ltd. (Shanghai, China). The sequences of PNA and oligonucleotides are listed in **Table S1.**

These PNA, MCH, DNA, Zr^{4+}, HA, BMP, EDC, NHS, DEA, $CuBr_2$, Me_6TREN and FMMA solutions were prepared with H_2O, 70% ethanol, 0.1 M phosphate buffer saline (PBS, pH 7.4), 10% ethanol, H_2O, DMSO, DMSO, DMSO, H_2O, DMF, DMF and DMF, respectively.

2.2 Apparatus

All electrochemical measurements were performed at room temperature (~25 °C). Electrochemical impedance spectroscopy (EIS) was tested in 0.1 M KNO_3 solution containing 5 mM $[Fe(CN)_6]^{4-/3-}$ (equimolar) and recorded using Autolab PGSTAT204 (Eco Chemie, Netherlands) in the frequency range of 0.1 MHz to 0.1 Hz with an amplitude of 5 mV. Cyclic voltammetry (CV), amperometric i–t curve (i–t), linear sweep voltammetry (LSV) and square wave voltammetry (SWV) were conducted on a CHI 760E electrochemical workstation (Shanghai CH Instruments Inc, China). Atomic force microscopy (AFM) images were obtained using a Dimension Icon (Bruker Nano Inc, USA). Scanning electron microscopy (SEM) images were obtained using a Sigma HD field emission SEM (Zeiss, Germany).

2.3 Fabrication of DNA biosensor based on HA and eATRP amplification

Prior to immobilization, bare gold electrode (2 mm in diameter) was polished to a mirror-like surface using Al_2O_3 slurries (0.3 and 0.05 μm, respectively) and successively rinsed ultrasonically with anhydrous ethanol and water. After immersing in piranha solution (30% H_2O_2 and 98% H_2SO_4, 1:3 v/v) for 15 min and rinsing with water, it was further electrochemically cleaned in freshly prepared 0.5 M H_2SO_4 solution via CV (potential range: -0.3~1.5 V and scan rate: 0.2 V s^{-1}) until a reproducible CV was obtained. Finally, it was ultrasonically washed with water and dried with nitrogen stream.

5 μL of PNA (0.5 μM) was dropped onto the electrode surface and incubated at 37 °C for 2.0 h. After washing with water to remove the non-specifically absorbed PNA, the modified electrode (PNA/Au) was immersed in 400 μL of MCH (2 mM) at 37 °C for 30 min to closure unoccupied binding sites. It was washed with 70% ethanol and water, which was denoted as MCH/PNA/Au. Following this, 10 μL of tDNA was added onto the electrode surface, after incubating at 37 °C for 1.5 h and moderately rinsing with PBS (0.1 mM, pH 7.4) solution to remove unhybridized tDNA (dsDNA was incubated with

PNA at 80 °C for 5 min and then incubated at 37 °C for 1.5 h). After that, the electrode was soaked in 400 µL of Zr^{4+} (5 mM) at 37 °C for 15 min and washing with 10% ethanol and water. The obtained electrode (Zr^{4+}/tDNA/MCH/PNA/Au) was further incubated at 37 °C for 40 min by pipetting 10 µL HA (10 µM) onto the electrode surface and rinsed with water (it was denoted as HA/Zr^{4+}/tDNA/MCH/PNA/Au). Then, the electrode was immersed in 400 µL of mixture (1 mM activated BMP and 1 mM DEA) at 37 °C for 1 h and rinsed with DMSO and water, which was denoted as BMP/HA/Zr^{4+}/tDNA/MCH/PNA/Au. In which activated BMP (aBMP) solution was obtained by adding equimolar EDC, NHS, BMP and reacting at 37 °C for 3.0 h (Nie et al., 2016).

The BMP-attached electrode was soaked in the polymerization mixture (freshly prepared by orderly adding 1.5 mL KBr (1 M), 10.5 mL KPF_6 (0.1 mM), 150 µL of FMMA (10 mM) and 90 µL of CuBr/Me_6TREN (10 mM, 1:1.2 in molarity) into 2760 µL of DMF) and electrochemically polymerized for 30 min using i–t curve under a properly negative potential. Subsequently, the electrode was treated with LSV (scan rate: 1.0 V s^{-1}, initial potential: 0 V and final potential: 0.25 V) and washed with DMF and water to eliminate adsorbed components (Cu^0 and FMMA); the resulting electrode was noted as FMMA/BMP/HA/Zr^{4+}/tDNA/MCH/PNA/Au. Finally, the prepared electrode was immersed in $LiClO_4$ (1 M) and measured using SWV (potential amplitude: 0.025 V, increase potential: 4 mV and quiet time: 30 s).

3. Results and discussion

3.1 Principle of the electrochemical biosensor for CYFRA 21-1 DNA detection

This ultrasensitive electrochemical DNA biosensor is constructed by utilizing polysaccharide and eATRP as the dual signal amplification technology and neutral PNA as CYFRA 21-1 DNA recognizing probes. The principle of CYFRA 21-1 DNA detection is illustrated in **Scheme 1A**. Initially, PNA probes are fixed onto the electrode surface

through self-assembly of Au–S bond. Through hybridization reaction, the CYFRA 21-1 DNA phosphate sites can be carried to the electrode surface and react with the carboxyl groups of HA by carboxylate-Zr^{4+}-phosphate chemistry. Due to the large number of hydroxyl groups in HA, it can provide more recognition sites for eATRP initiators. After that, multiple initiators of eATRP, BMP, are tightly attached to the HA backbone by esterification reaction. Through eATRP using FMMA as the monomer, large numbers of electro-active polymers are grafted in situ from the established functionalized HA initiation sites, which markedly amplifies the electrochemical signal. In this study, polymerization is controlled by applying an appropriate potential at the work electrode. The specified principle of eATRP is illustrated in **Scheme 1B**. First, through the application of an electrochemical potential at the initiators-attached electrode, the catalytic complex ($Br–Cu^{II}/Me_6TREN^+$) is electrochemically reduced to its active complex ($Br–Cu^{I}/Me_6TREN$), which can partially dissociate to Br^- and Cu^{I}/Me_6TREN^+ (Pan et al., 2018). By inner sphere electron transfer, the latter reacts with the initiator ($P_n–Br$) to produce radicals ($P_n^{\bullet}$) and deactivators ($Br–Cu^{II}/Me_6TREN^+$), which are again involved in catalytic cycling. The radicals can propagate by the monomers (FMMA), terminate (P_nP_m) or be deactivated back to the dormant species (P_n-Br) by higher oxidation state catalyst ($Br–Cu^{II}/Me_6TREN^+$) through outer sphere electron transfer (Chmielarz et al., 2017). Then the coupled radicals (P_nP_m) react with $Br–Cu^{II}/Me_6TREN^+$ to form long polymeric chains ($P_nP_m–X$). By taking advantage of efficient signal amplification of the functionalized HA and electrochemically mediated polymerization, a large number of FMMA-labelled polymeric chains are grafted from each tDNA phosphate site, thereby significantly improving the sensitivity of the biosensor for CYFRA 21-1 DNA detection.

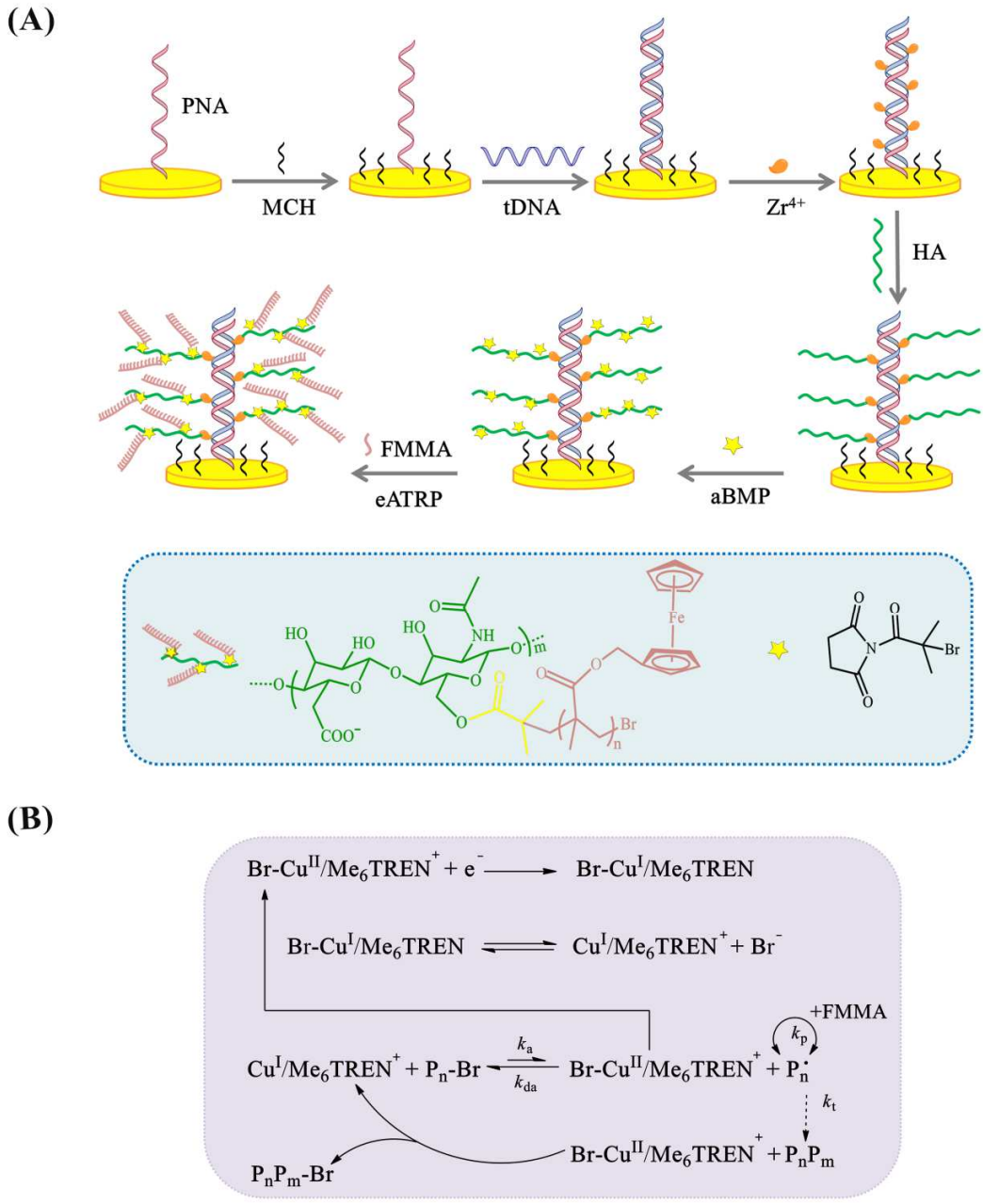

Scheme 1. (A) Schematic illustration of the fabricated DNA biosensor based on polysaccharide and eATRP dual signal amplification. (B) Principle of the eATRP-based amplification strategy (P_n–Br = alkyl bromide, k_a = activation rate constant, k_{da} = deactivation rate constant, k_p = propagation rate constant and k_t = termination rate constant).

3.2 Feasibility of electrochemical biosensor for CYFRA 21-1 DNA detection

In eATRP, an applied potential (E_{app}) is used to electrochemically reduce the deactivator ($X-Cu^{II}L$) to its activator ($Cu^{I}L$), thereby triggering controlled radical polymerization (Ribelli et al., 2019). Therefore, the choice of E_{app} prior to the electrochemical polymerization is of primary importance. As shown in **Fig. 1A**, E_{app} was investigated by the CV (potential range: −0.8 V ~ 0.5 V and scan rate: 0.1 V s^{-1}) of BMP/HA/Zr^{4+}/tDNA/MCH/PNA/Au in a FMMA-free polymerization solution. The cathode peak at −0.54 V represents $Cu^{II}Br_2$/Me_6TREN is reduced to $Cu^{I}Br$/Me_6TREN.

$$R_p = k_p[M][P_n^{\cdot}] = k_p K_{ATRP} \frac{[Cu^{I}L][P_n\text{–}X][M]}{[Cu^{II}L]} \quad (1)$$

$$E_{app} = E_{1/2} + \frac{RT}{F} \ln \frac{[X\text{–}Cu^{II}L]}{[X\text{–}Cu^{I}L]} \quad (2)$$

According to the Equations 1 and 2 (Chmielarz et al., 2017; Magenau et al., 2013; Pan et al., 2018), the polymerization rate (R_p) is directly proportional to the $[Cu^{I}L]/[X–Cu^{II}L]$. The $[X–Cu^{II}L]/[X–Cu^{I}L]$ ratio can be modulated by changing the overpotential, η (η = $E_{app}–E_{1/2}$; $E_{1/2}$ is the half-wave potential of $X–Cu^{II}L$ and $X–Cu^{I}L$). Therefore, changing E_{app} causes an alteration in R_p. A more negative E_{app} produces other undesired electron transfer effect (e.g. reduction of the activator $Cu^{I}L$ to Cu^{0} and L^{-}) and reduces the rate of deactivation, resulting in slightly higher dispersity. However, a more positive E_{app} is believed to quickly oxidize Cu^{I}/L to Cu^{II}/L deactivators, which can rapidly stop the polymerization reaction. Therefore, an E_{app} value of −0.54 V was selected.

To validate the feasibility of the fabricated biosensor for tDNA detection, electrodes prepared by different methods were measured by SWV. As shown in **Fig. 1B**, no distinct current signal can be observed (except for a weak background signal) in the absence of either one of PNA (curve a), tDNA (curve b), Zr^{4+} (curve c), BMP (curve d) or eATRP solution (curve f). On the contrary, a weak oxidation peak is detected in the absence of HA (curve e) at a potential of ~ 0.3 V, corresponding to the oxidation of FMMA tags (Hu et al., 2018). This indicates that by utilizing only the strong coordination between Zr^{4+} ions and phosphate and carboxylic acid groups, ATRP initiators can be introduced for electrochemical polymerization to generate an amplified electrochemical signal. For

FMMA/BMP/HA/Zr^{4+}/tDNA/MCH/PNA/Au (curve f), a significant oxidation peak is clearly observed, indicating that the attachment of HA can provide more active sites for the initiators, thereby triggering more polymerization chain reactions and further amplifying the electrochemical signal. These results clearly demonstrate the feasibility of using polysaccharide and eATRP dual signal amplification for DNA detection. Moreover, the electrochemistry of newly formed electro-active polymers was investigated through CV at different scan rates. As illustrated in **Fig. 1C**, the redox current is proportional to scan rate from 0.01 to 0.5 V s^{-1}, confirming that the polymers are tethered to the electrode surface (Grabowska et al., 2014; Hu et al., 2017).

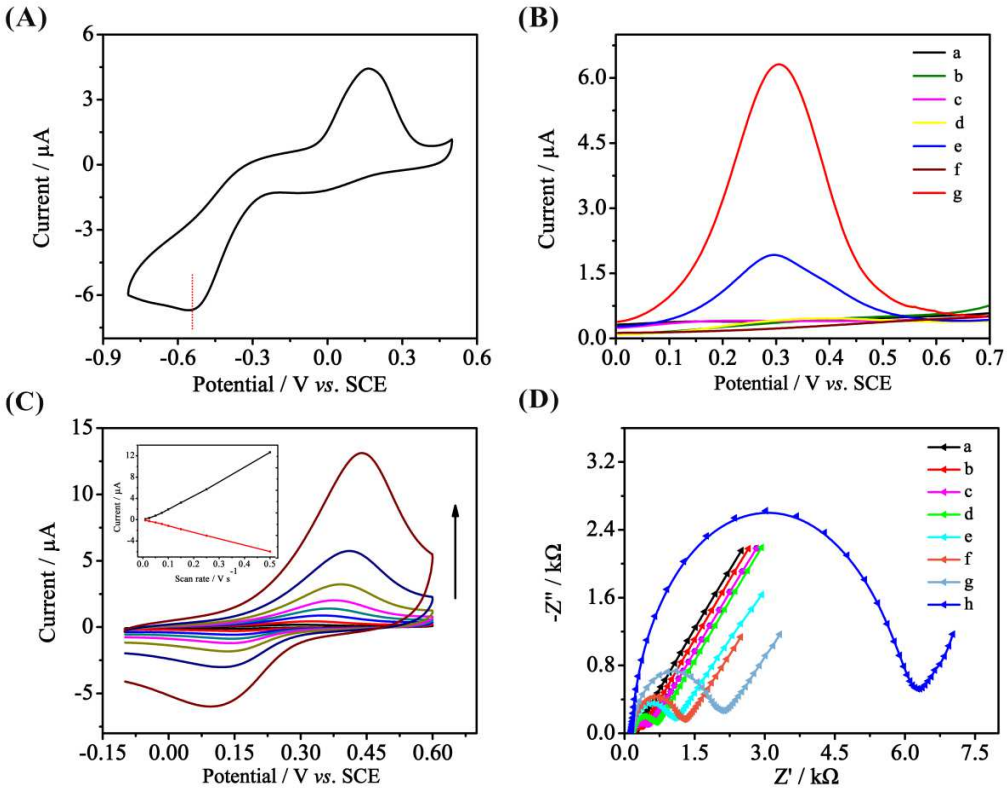

Fig. 1. (A) CV curve of BMP/HA/Zr^{4+}/tDNA/MCH/PNA modified electrode in FMMA-free polymerization solution (scan rate: 0.1 V s^{-1}). (B) SWV curves of FMMA/BMP/HA/Zr^{4+}/tDNA/MCH/PNA/Au (g) in the absence of PNA (a), tDNA (b), Zr^{4+} (c), BMP (d), HA (e) or eATRP solution (f). (C) CV curves of FMMA/BMP/HA/Zr^{4+}/tDNA/MCH/PNA/Au at

scan rates from 0.01 to 0.5 V s^{-1}. Inset shows the correlation of oxidation (marked black) and reduction (marked red) peak current with the scan rate. (D) Nyquist plots of Au (a), PNA/Au (b), MCH/PNA/Au (c), tDNA/MCH/PNA/Au (d), Zr^{4+}/tDNA/MCH/PNA/Au (e), HA/Zr^{4+}/tDNA/MCH/PNA/Au (f), BMP/HA/Zr^{4+}/tDNA/MCH/PNA/Au (g) and FMMA/BMP/HA/Zr^{4+}/tDNA/MCH/PNA/Au (h). The concentrations of tDNA were all 1 pM.

3.3 Characterizations

The assembly process for the electrochemical DNA biosensor was characterized by EIS owing to its relatively high sensitivity to subtle changes in the electrode surface. **Fig. 1D** shows that the typical Nyquist plots comprised a semicircle at high frequency related to the charge-transfer resistance and linear component at low frequency associated with the diffusion process. The diameter of the semicircle is equal to the charge-transfer resistance (R_{ct}), corresponding to the restricted diffusion of the redox probe (e.g. $[Fe(CN)_6]^{3-/4}$) accessing the interface layer (Wang et al., 2015). It was observed that the impedance spectrum of the bare gold electrode has a relatively small semicircle (~0.20 kΩ, curve a). The assembly of PNA (~0.36 kΩ, curve b) and MCH (~0.47 kΩ, curve c) results in a gradual increase in R_{ct} due to the poor electron transfer efficiency of the monolayer (Hu et al., 2018). After the hybridization of PNA and tDNA, R_{ct} further increases (~0.65 kΩ, curve d) as a result of the electrostatic repulsion between DNA phosphorylated sites and $[Fe(CN)_6]^{3-/4-}$. Interestingly, the chelation of Zr^{4+} ions (~1.10 kΩ, curve e) with phosphorylation sites also raises R_{ct}; since Zr^{4+} ions can adsorb $[Fe(CN)_6]^{3-/4-}$ and then pre-adsorbed $[Fe(CN)_6]^{3-/4-}$ has an electrostatic repulsion effect on the incoming $[Fe(CN)_6]^{3-/4-}$ (Hu et al., 2019). Similarly, after the immobilization of HA (~1.26 kΩ, curve f), R_{ct} increases due to electrostatic repulsion of HA carboxylic acid groups towards $[Fe(CN)_6]^{3-/4-}$. Subsequently, the attachment of BMP (~2.10 kΩ, curve g) increases R_{ct} because the modified initiators reduce the surface hydrophilicity and prevent the redox probe from accessing the electrode surface. Lastly, because of the formation of

highly hydrophobic polymeric chains, the eATRP reaction causes a distinct increase in R_{ct} (~6.26 kΩ, curve h). Notably, plenty of electro-active polymers are labelled on the electrode but do not promote charge-transfer, which is mainly attributed to the FMMA molecules attached to the polymer chain not being conjugated to each other (Sato et al., 2018); therefore the electrons at the centre of FMMA are not delocalized. These results clearly indicate the successful fabrication of the DNA biosensor.

The biosensor fabrication process was further characterized through AFM and SEM. **Fig. 2A** shows the morphology of tDNA/MCH/PNA/Au and the surface height is 11.4 nm. A taller image with a surface height of 17.2 nm was obtained after HA was attached to the electrode surface (**Fig. 2B**). **Fig. 2C** depicts the surface morphology of the initiator-coated electrode with a surface height of 24.7 nm after polymerisation in a 0.06 mM FMMA mixture. Analogously, the morphology of tDNA/MCH/PNA modified electrode is relatively smooth (**Fig. 2D**). When HA is immobilized onto the electrode surface, few polymer particles are present on the electrode surface (**Fig. 2E**). Following the eATRP reaction, a large amount of polymers are densely dispersed on the electrode surface (**Fig. 2F**). These experimental results clearly confirm that the biosensor based on polysaccharide and eATRP dual amplification was successfully constructed.

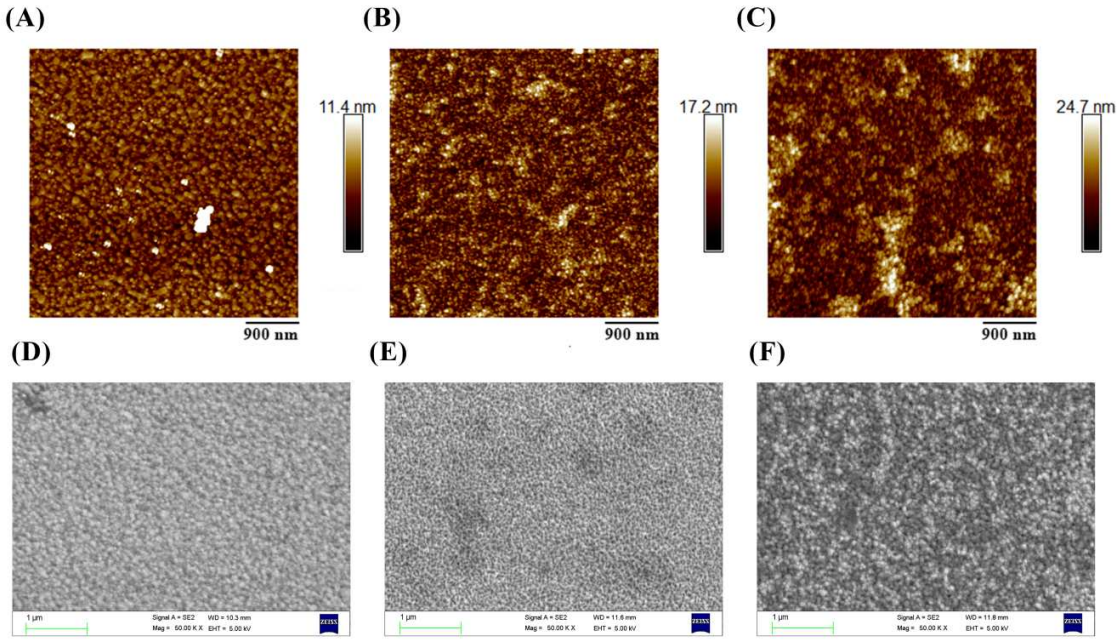

Fig. 2. AFM images of the (A) tDNA/MCH/PNA/Au, (B) HA/Zr^{4+}/tDNA/MCH/PNA/Au and (C) FMMA/BMP/HA/Zr^{4+}/tDNA/MCH/PNA/Au. SEM images of the (C) tDNA/MCH/PNA/Au, (D) HA/Zr^{4+}/tDNA/MCH/PNA/Au and (E) FMMA/BMP/HA/Zr^{4+}/tDNA/MCH/PNA/Au.

3.4 Optimal conditions for the fabricated biosensor

In the process of electrochemical biosensor fabrication, important parameters should be optimized to improve the efficiency and sensitivity of the sensor.

For the proposed biosensor, the intensity of oxidation current correlates with the amount of FMMA labels on the electrode surface. eATRP offers the capability of tuning the length of the grafted polymer chains by varying the polymerization time. That is, a longer polymerization time leads to more FMMA tags on the electrode surface. **Fig. 3(A)** shows the variation between polymerization time and oxidation current of the CV curves. The current signal increases rapidly with polymerization time for the first 20 min **(Fig. 3(B))**. Subsequently, it grows slowly until it reaches a plateau at 30 min, which may be caused by poor electron transfer efficiency or radical termination (Yuan et al., 2011). Therefore, the optimal polymerization time was chosen as 30 min.

Due to the unique molecular structure and physicochemical properties of HA, it provides more recognition sites for the initiators of the polymerization reaction, which can significantly improve subsequent polymerization. Therefore, the HA reaction time is an important factor in the biosensor sensitivity. As can be seen from Fig. **3(C)**, the current signal increases until it reaches a plateau at 40 min, indicating that the connected HA is saturated at 40 min. Therefore, 40 min was selected as the optimal time of HA incubation.

The catalyst used in eATRP plays a crucial role because it controls on the amount of radicals generated, inhibiting the termination of the polymer chain and to ensure sufficient growth of the polymer chain. In this context, the effect of $CuBr_2/Me_6TREN$ concentration on eATRP was investigated from 10 to 100 μM. As shown in **Fig. 3(D)**, the current signal gradually increases with an increase in the catalyst concentration, reaching a maximum at 60 μM. This is because as the concentration of $CuBr_2/Me_6TREN$ increases, the reduction of Cu^{II} to Cu^{I} gradually increases, leading to the more polymerization of radicals. Subsequently, due to the low initiator density and high deactivation rate, the current signal decreases as $CuBr_2/Me_6TREN$ concentration further increases. Consequently, the concentration of $CuBr_2/Me_6TREN$ was set to 60 μM in the following experiment.

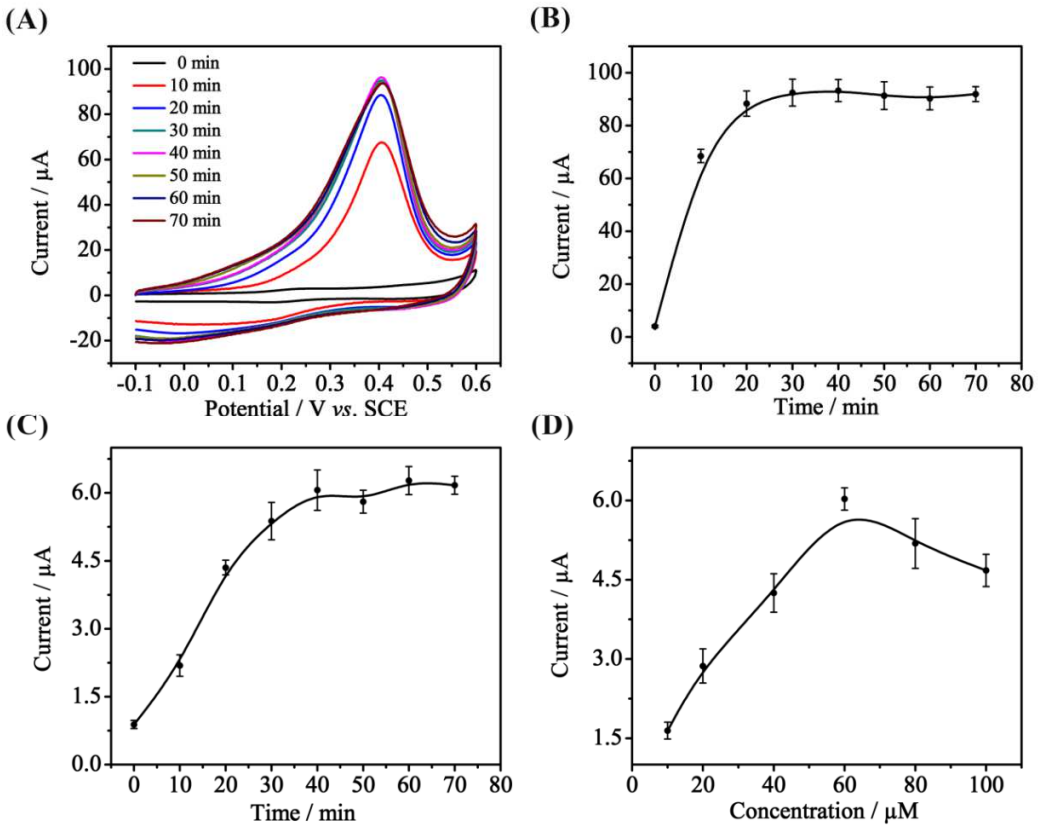

Fig. 3. (A) CV curves of BMP/HA/Zr^{4+}/tDNA/MCH/PNA/Au in eATRP mixture (scan rate: 1.0 V s^{-1}). (B) Plot of peak current with eATRP time. The effect of HA reaction time (C) and $CuBr_2$/Me_6TREN concentration (D) in relation to electrochemical signal. The concentrations of tDNA were all 1 pM. Error bars are the standard deviations of three individual measurements.

3.5 Analytical performance

Under optimized conditions, electrochemical experiments were performed to quantitatively evaluate the response range and the limit of detection (LOD) of the electrochemical biosensor for tDNA detection. **Fig. 4** shows a good linearity between the current signal and logarithm of tDNA concentration ranging from 100 aM to 100 pM. The corresponding regression equation is I (μA) = 0.89 log [C_{tDNA}/fM] + 3.75 (R^2 = 0.994) and the LOD is calculated to be 9.04 aM (equivalent to ~54 molecules in a 10 μL sample) based on S/N = 3 (where S represents the standard deviation of the control and N

represents the slope of regression equation). Through the comparison of analytical performance between the proposed DNA biosensor and those reported previously (**Table S2**), the established sensor exhibits a comparable or superior linear range and LOD.

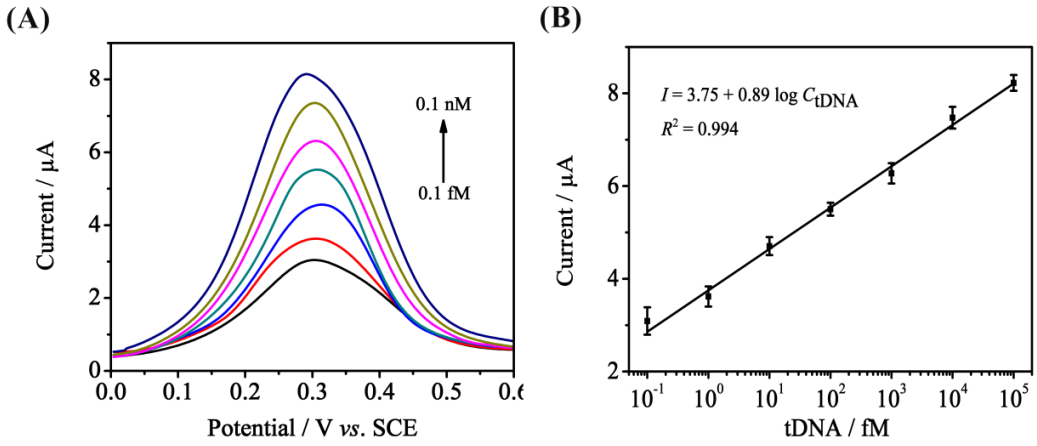

Fig. 4. (A) SWV curves of different concentrations of tDNA. The concentrations of tDNA were 0.1, 1, 10, 10^2, 10^3, 10^4, and 10^5 fM respectively. (B) Linear correlation curve between current signal and logarithm of different tDNA concentrations. Error bars are the standard deviations of three individual measurements.

3.6 Selectivity, reproducibility, stability and anti-interference ability of the electrochemical biosensor

Under the same experimental conditions, we tested the electrochemical signal to tDNA, SBM, TBM and NC to demonstrate the selectivity of the proposed method. The concentration of all DNA fragments was 1 pM. As can be seen from **Fig. 5(A)**, the electrochemical signal of SBM is 29.2% that of tDNA, demonstrating that the DNA biosensor can effectively discriminate SBM. The electrochemical signals of TBM and NC are approximately 76.8% and 85.5% lower than that of tDNA. These results indicate that the prepared biosensor is highly selective for tDNA detection.

Moreover, the reproducibility of the biosensor was investigated based on the intra- and inter-assays (n = 5). The relative standard deviations of the intra- and inter-assays are

3.2% and 3.8%, respectively, indicating that the fabricated electrochemical biosensor has high reproducibility. To evaluate the stability of the electrochemical biosensor, five identically modified electrodes were prepared and stored in 4 degree refrigerator. After one month, it was observed that up to 93.0% of current signal could be retained. Thus, the electrochemical biosensor is satisfactorily stable during storage.

To evaluate the anti-interference capability of the sensor, we studied the electrochemical signal of tDNA in 10% human serum samples. A certain number of tDNA were injected into 10% serum to prepare a serum sample. The corresponding current signal in the 10% serum sample is compared with the current signal in 0.1 M PBS. As shown in **Fig. 5(B)**, the current signal of the 10% serum samples respectively is 91.8%, 88.2% and 82.9% of those from 1 pM, 10 fM and 0.1 fM tDNA in 0.1 M PBS. Consequently, the electrochemical biosensor has good anti-interference capability in serum samples, suggesting its significant clinical application potential.

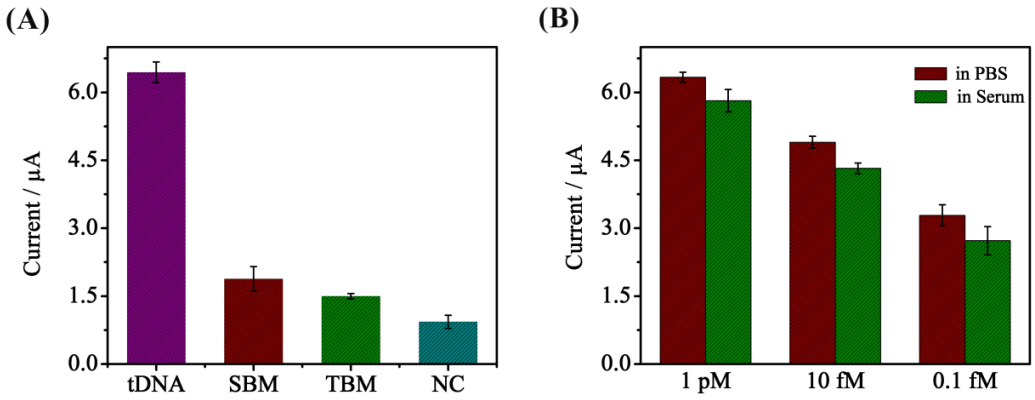

Fig. 5. (A) Current intensity of the biosensor toward the complementary CYFRA 21-1 DNA (tDNA, 1 pM), single-base mismatched DNA (SBM, 1 pM), three-base mismatched DNA (TBM, 1 pM) and non-complementary DNA (NC, 1 pM). (B) Current intensity of the biosensor in 0.1 M PBS (pH 7.4) and 10% serum samples. Error bars are the standard deviations of three individual measurements.

3.7 Proposed electrochemical biosensor for double-stranded CYFRA 21-1 DNA detection

Currently, most reported DNA sensors are available for ssDNA, but not direct detection of dsDNA. In fact, the target DNA in its natural state is double stranded, which requires the denaturation of ssDNA into dsDNA prior to analysis. This significantly limits the applications scope of biosensor technology. PNA has the ability to invade a DNA/DNA duplex to form specific PNA/DNA complexes (Lee et al., 2014). As such, the proposed detection assay can also be used in the direct detection of dsDNA. As shown in **Fig. S1,** the current signal is linear with the dsDNA concentration in the range of 1.0 fM to 0.1 nM with a LOD of 0.14 fM. Moreover, the selectivity and anti-interference capability of the sensor to dsDNA detection were evaluated. As illustrated in **Fig. S2(A)**, the current signal of dsDNA is much higher than those of mismatched dsDNA. This demonstrates that the biosensor has the potential to discriminate single-base mismatch. As shown in **Fig. S2(B)**, the current signals generated by 0.1 nM, 1 pM and 10 fM dsDNA in the 10% serum samples are 92.9%, 86.1% and 81.8% in 0.1 M PBS, respectively. These results confirm that the dual signal amplification method via polysaccharide and eATRP can also be applied to the direct detection of dsDNA.

4. Conclusions

We have developed an ultrasensitive electrochemical biosensor for CYFRA 21-1 DNA detection based on polysaccharide and eATRP dual signal amplification. Under optimized conditions, the biosensor can detect as low as 9.04 aM and 0.14 fM as the detection limit, respectively for ssDNA and dsDNA. Moreover, this biosensor can specifically discriminate mismatched bases and detect CYFRA 21-1 DNA in serum samples. Further studies need to be conducted to shorten the analysis time of actual samples. This signal amplification strategy can be readily extended to the ultrasensitive detection of other biomarkers, such as proteins and miRNAs.

Acknowledgements

This work was supported by four funds: The National Key Research and Development Project (The Major Project for Research of the Modernization of TCM): Key Technology Research for the Characteristic Chinese Medicine Industry Chain of Rehmannia glutinosa (2017YFC1702800); The Major Science and Technology Projects in Henan Province: Study on the key technology for quality control and the key characteristics of Rehmannia glutinosa, Dioscorea opposita Thunb and Achyranthes bidentata Blume from Henan Province (171100310500); The project of tackling of key scientific and technical problems in Henan Province (192102310033); National Natural Science Foundation of China (21974068).

Declaration of interests

The authors declare that they have no known competing financial interests or personal relationships that could have appeared to influence the work reported in this paper.

References

Allen, Z.T., Sackey-Addo, J.R., Hopps, M.P., Tahseen, D., Anderson, J.T., Graf, T.A., Cooley, C.B., 2019. Chem. Sci. 10, 1017-1022.

Arya, S.K., Bhansali, S., 2011. Chem. Rev. 111, 6783-6809.

Cedres, S., Nunez, I., Longo, M., Martinez, P., Checa, E., Torrejon, D., Felip, E., 2011. Clin. Lung Cancer 12, 172-179.

Chen, M., Wang, Y., Su, H., Mao, L., Jiang, X., Zhang, T., Dai, X., 2018. Sens. Actuators, B 255, 2910-2918.

Chmielarz, P., Fantin, M., Park, S., Isse, A.A., Gennaro, A., Magenau, A.J.D., Sobkowiak, A., Matyjaszewski, K., 2017. Prog. Polym. Sci. 69, 47-78.

Grabowska, I., Singleton, D.G., Stachyra, A., Gora-Sochacka, A., Sirko, A., Zagorski-Ostoja, W., Radecka, H., Stulz, E., Radecki, J., 2014. Chem. Commun. 50, 4196-4199.

Han, K.C., Yang, E.G., Ahn, D.R., 2013. Biosens. Bioelectron. 50, 421-424.

He, P., Lou, X., Woody, S.N., He, L., 2019. ACS Sens. 4, 992-1000.

Hu, Q., Han, D., Gan, S., Bao, Y., Niu, L., 2018. Anal. Chem. 90, 12207-12213.

Hu, Q., Kong, J., Han, D., Zhang, Y., Bao, Y., Zhang, X., Niu, L., 2019. Anal. Chem. 91, 1936-1943.

Hu, Q., Wang, Q., Sun, G., Kong, J., Zhang, X., 2017. Anal. Chem. 89, 9253-9259.

Hu, W., Bi, Z.Y., Chen, Z.L., Liu, C., Li, L.L., Zhang, F., Zhou, Q., Zhu, W., Song, Y.Y., Zhan, B.T., Zhang, Q., Bi, Y.Y., Sun, C.C., Li, D.J., 2018. Cancer Lett. 427, 18-27.

Jones, G.R., Anastasaki, A., Whitfield, R., Engelis, N., Liarou, E., Haddleton, D.M., 2018. Angew. Chem., Int. Ed. 57, 10468-10482.

Kim, M.S., Kwon, S., Kim, T., Lee, E.S., Park, J.K., 2011. Biomaterials 32, 1396-1403.

Lee, J., Park, I.S., Jung, E., Lee, Y., Min, D.H., 2014. Biosens. Bioelectron. 62, 140-144.

Leophairatana, P., Samanta, S., De Silva, C.C., Koberstein, J.T., 2017. J. Am. Chem. Soc. 139, 3756-3766.

Li, Z.B., Miao, X.M., Xing, K., Zhu, A.H., Ling, L.S., 2015. Biosens. Bioelectron. 74, 687-690.

Magenau, A.J.D., Bortolamei, N., Frick, E., Park, S., Gennaro, A., Matyjaszewski, K., 2013. Macromolecules 46, 4346-4353.

Magenau, A.J.D., Strandwitz, N.C., Gennaro, A., Matyjaszewski, K., 2011. Science 332, 81-84.

Nie, J.J., Zhao, W., Hu, H., Yu, B., Xu, F.J., 2016. ACS Appl. Mater. Interfaces 8, 8376-8385.

Pan, X.C., Fantin, M., Yuan, F., Matyjaszewski, K., 2018. Chem. Soc. Rev. 47, 5457-5490.

Pujol, J.L., Grenier, J., Daures, J.P., Daver, A., Pujol, H., Michel, F.B., 1993. Cancer Res. 53, 61-66.

Qian, H., He, L., 2010. Sens. Actuators, B 150, 594-600.

Ribelli, T.G., Lorandi, F., Fantin, M., Matyjaszewski, K., 2019. Macromol. Rapid Commun. 40, e1800616.

Sato, K., Ichinoi, R., Mizukami, R., Serikawa, T., Sasaki, Y., Lutkenhaus, J., Nishide, H., Oyaizu, K., 2018. J. Am. Chem. Soc. 140, 1049-1056.

Seidi, F., Salimi, H., Shamsabadi, A.A., Shabanian, M., 2018. Prog. Polym. Sci. 76, 1-39.

Shen, Q., Han, L., Fan, G., Zhang, J.R., Jiang, L., Zhu, J.J., 2015. Anal. Chem. 87, 4949-4956.

Srinivas, P.R., Kramer, B.S., Srivastava, S., 2001. Lancet Oncol. 2, 698-704.

Sun, Y., Du, H., Lan, Y., Wang, W., Liang, Y., Feng, C., Yang, M., 2016. Biosens. Bioelectron. 77, 894-900.

Wang., J.-S., Matyjaszewsk., K., 1995. J. Am. Chem. Soc. 117, 5614-5615.

Wang, T., Zhang, Z., Li, Y., Xie, G., 2015. Sens. Actuators, B 221, 148-154.

Xing, X., Liu, S., Yu, J., Lian, W., Huang, J., 2012. Biosens. Bioelectron. 31, 277-283.

Yang, C.T., Pourhassan-Moghaddam, M., Wu, L., Bai, P., Thierry, B., 2017. Acs Sens. 2, 635-640.

Yuan, L, Wu, Y., Shi, H., Liu, S., 2011. Chem. Eur. J. 17, 976-983.

Zeng, Y., Bao, J., Zhao, Y., Huo, D., Chen, M., Qi, Y., Yang, M., Fa, H., Hou, C., 2018. Bioelectrochemistry 120, 183-189.

Zhao, Q., Piao, J., Peng, W., Wang, Y., Zhang, B., Gong, X., Chang, J., 2018. ACS Appl. Mater. Interfaces 10, 3324-3332.

Highlights

- A novel electrochemical biosensor is developed for ultrasensitive detection of CYFRA 21-1 DNA.
- A detection limit of 9.04 aM is achieved based on polysaccharide and eATRP dual amplification.
- The proposed sensor shows high sensitivity, selectivity, low cost and friendly environment.
- This strategy may hold great potential in biomedical research and clinical diagnosis.

Declaration of Interest Statement

The authors declare that they have no known competing financial interests or personal relationships that could have appeared to influence the work reported in this paper.